Alkene Isomerization using a Heterogeneous Nickel-Hydride Catalyst

Alison Sy-min Chang, Melanie A. Kascoutas, Quinn P. Valentine, Kiera I. How, Rachel M. Thomas, and Amanda K. Cook*

Department of Chemistry and Biochemistry, University of Oregon, Eugene, OR 97403, United States

ABSTRACT: Transition metal-catalyzed alkene isomerization is an enabling technology used to install an alkene distal to its original site. Due to their well-defined structure, homogeneous catalysts can be fine-tuned to optimize reactivity, stereoselectivity, and positional selectivity, but they often suffer from instability and non-recyclability. Heterogeneous catalysts are generally highly robust but continue to lack active-site specificity and are challenging to rationally improve through structural modification. Known single-site heterogeneous catalysts for alkene isomerization utilize precious metals and bespoke, expensive, and synthetically intense supports. Additionally, they generally have mediocre reactivity, inspiring us to develop a heterogeneous catalyst with an active site made from readily available compounds made of Earth-abundant elements. Previous work demonstrated that a very active homogeneous catalyst is formed upon protonation of $Ni[P(OEt)_3]_4$ by H_2SO_4, generating a $[Ni–H]^+$ active site. This catalyst is incredibly active, but also decomposes readily, which severely limits its utility. Herein we show that by using a solid acid (sulfated zirconia, SZO_{300}), not only is this decomposition prevented, but high activity is maintained, improved selectivity is achieved, and a broader scope of functional groups is tolerated. Preliminary mechanistic experiments suggest that the catalytic reaction likely goes through an intermolecular, two-electron pathway. A detailed kinetic study comparing the state-of-the-art Ni and Pd isomerization catalysts reveals that the highest activity and selectivity is seen with the Ni/SZO_{300} system. The reactivity of Ni/SZO_{300}, is not limited to alkene isomerization; it is also a competent catalyst for hydroalkenylation, hydroboration, and hydrosilylation, demonstrating the broad application of this heterogeneous catalyst.

INTRODUCTION

Transition metal-catalyzed alkene isomerization is an appealing approach to reposition an alkene within a molecule (Figure 1a).[1,2] Significant advancements in the field of homogeneously catalyzed isomerization have been made,[3–5] but efficient and selective heterogeneous catalysts for isomerization remain sparse, despite the potential to apply the advantages of heterogeneous catalysis (recyclability, added stability, complementary selectivity).[6,7] Currently, this area of catalysis is severely underdeveloped and dominated by the use of precious metals, specialty organic polymers as supports, and ill-defined active sites in nanoparticles. Notable examples of single-site catalysts include works by Ley,[8] Grotjahn,[9] and Jia[10] which immobilize Ir, Ru, or Rh complexes, respectively, onto ligand-modified organic polymers (Figure 1b). These systems display good catalyst recyclability, but at the expense of reduced catalytic activity and/or *E*/*Z*-selectivity in comparison to their homogeneous analogues. Many nanoparticle-based catalysts for alkene isomerization are known, but because of their crude synthesis methods (*e.g.*, treatment under hydrogen at elevated temperatures), the active sites are unknown, making structure-activity relationships challenging to elucidate (Figure 1b, top right).[11,12] Likely because of this lack of control in the synthesis, the activity and selectivity of the catalysts tend to be low. Because the structure of single-site catalysts can be designed and systematically modified, they have the potential to control, understand, and improve reactivity.[7,13]

A pivot towards more precise methods to prepare heterogeneous catalysts bearing well-defined active sites grants the ability to develop structure–activity relationships and encourages further catalyst development. Strategies to synthesize single-site catalysts include the surface organometallic chemistry (SOMC) approach[14] and the use of metal-organic and covalent organic frameworks (MOFs and

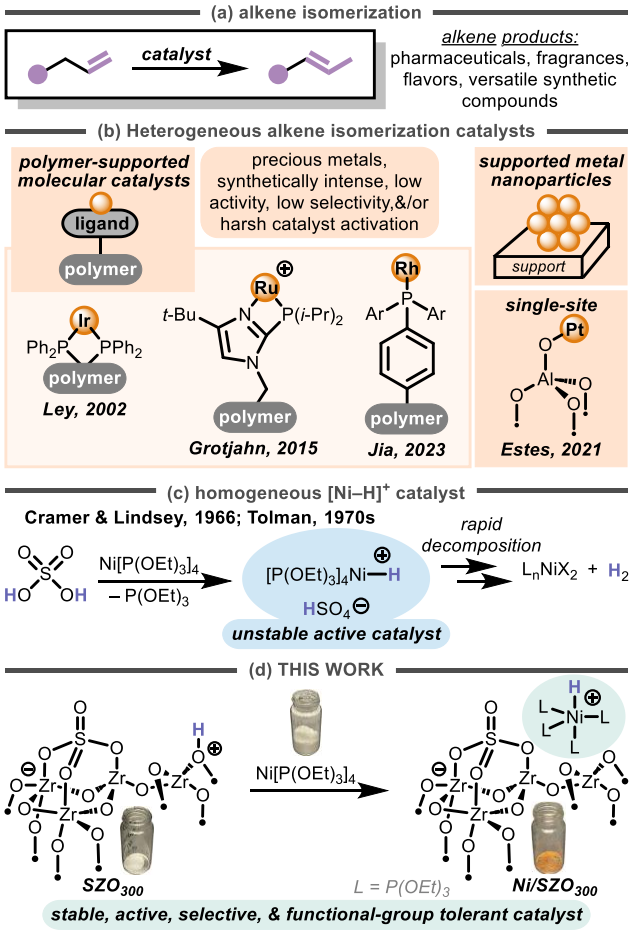

Figure 1. (a) Alkene isomerization. (b) Types of heterogeneous catalysts for alkene isomerization. (c) Ni/H_2SO_4 generation and decomposition. (d) This work: development of Ni/SZO_{300} for alkene isomerization.

https://doi.org/10.26434/chemrxiv-2023-rt2gt-v2 **ORCID:** https://orcid.org/0000-0003-3501-8502

COFs, respectively), and both have had limited success with alkene isomerization. Estes demonstrated that an alumina-supported platinum-hydride is effective at 1-hexene isomerization (Figure 1b, bottom right),[15] and a handful of examples of MOFs show activity for 1-butene isomerization and E/Z isomerization.[16–18] While these advancements demonstrate the potential of single-site catalysts in alkene isomerization, their substrate scopes are highly limited and often utilize precious metals as the active site.

SOMC is an evolving method that reaps the benefits of both homogeneous and heterogeneous catalysts. Typically, catalysts prepared using a SOMC approach deliver reactive species with molecular precision and enhanced stability compared to their homogeneous analogs. Select examples show marked catalytic improvement over their homogeneous analogs (*e.g.*, [W]/SiO_2–catalyzed alkene metathesis,[19] [Ir]/SiO_2–catalyzed methane borylation,[20] and [Hf]/sulfated zirconia-catalyzed ethylene/1-octene copolymerization),[21] demonstrating the potential of this approach.

Cramer and Lindsey found that Ni(0) in combination with sulfuric acid generates a highly active catalyst for alkene isomerization,[22] and Tolman studied the reaction's mechanism and the structure of the active catalyst.[23,24] A cationic Ni–H is proposed as the active catalyst, which forms from protonation of the Ni(0) center with the strong acid. This catalyst, while highly active, decomposes rapidly by a second equivalent of H^+, irreversibly forming an inactive Ni(II) species and H_2 (Figure 1c). We hypothesized that immobilization of the [Ni–H]$^+$ catalyst would prevent this decomposition, thereby improving catalyst stability and broadening its use in organic synthesis. Efforts to improve this catalyst's stability by means of heterogenization were performed using sulfated polymers;[25,26] this strategy improved the catalyst stability and recyclability, but at the expense of catalytic activity and alkene selectivity compared to the homogeneous catalyst (*vide infra*).

Using acidic metal oxides offers significant advantages over polymer-based supports, including ease and precision of synthesis and cost of materials.[27,28] Because of these advantages, the SOMC approach using acidic metal oxides has been taken to generate active catalysts for a wide variety of applications, such as hydrogenation,[29,30] ethylene (co)polymerization,[31,32,21] H/D exchange,[33,34] hydrogenolysis,[35] and alkane metathesis.[35] These active sites are generated by protonolysis or abstraction of an X-type ligand at the metal center, resulting in the active site being ionically tethered to the support, which is in contrast to the M–$O_{surface}$ bond that is formed with traditional SOMC approaches (e.g., see Estes example in Figure 1b). We hypothesized that the novel strategy of protonating metal centers with these strongly acidic metal oxides would be effective in generating immobilized [M–H]$^+$ species, which are broadly invoked as active sites in catalysis. In developing this method, the active site of the catalyst would be immobilized via an ionic bond between the active site complex, [Ni–H]$^+$, and the anionic support. Due to its straightforward nature, this SOMC approach also has the potential to inform future catalyst design and rationale for analogous systems. This strategy would be particularly useful in addressing the challenge of the decomposing [Ni–H]$^+$ catalyst for alkene isomerization.

In this report, we demonstrate that our novel approach is successful: the acidic metal oxide, sulfated zirconia (SZO_{300}) is an excellent proton source and support for generating a putative [Ni–H]$^+$ active site, which is highly active and selective catalysts for alkene isomerization (Figure 1d). We demonstrate that the catalyst, Ni/SZO_{300}, is compatible with a broad scope of alkenes including those containing functional groups with heteroatoms, halides, acid-labile groups, and electronically and sterically diverse groups. Recyclability and catalyst aging studies reveal enhanced catalyst stability. Notably, this heterogeneous catalyst shows marked improvements in stability, selectivity, and functional group tolerance in comparison to the homogeneous analog. Lastly, we show the versatility of this heterogeneous [Ni–H]$^+$ catalyst and have successfully applied it to various alkene hydrofunctionalization reactions.

RESULTS AND DISCUSSION

Optimization. We initiated our investigations using metal oxides as potential acid sources to generate [Ni–H]$^+$ species from protonation of Ni[P(OEt)$_3$]$_4$. We speculated that [Ni–H]$^+$ active sites could be formed by reacting this Ni^0 complex with isolated surface hydroxyls. A series of metal-oxide supports commonly used in SOMC, silica dehydroxylated at 700 °C ($SiO_{2\text{-}700}$), alumina dehydroxylated at 700 °C ($Al_2O_{3\text{-}700}$), and zirconia dehydroxylated at 700 °C ($ZrO_{2\text{-}700}$),[14,27] were screened for the isomerization of 4-allylanisole (**1a**) to anethole (**2a**), but all failed to demonstrate any desired reactivity (Table 1, entries 1-3). We postulated that the surface hydroxyls were not acidic enough to favorably generate the [Ni–H]$^+$ active species, so we tested a more acidic metal oxide, sulfated zirconia (SZO_{300}).[28,36] The catalyst is generated in situ from the combination of Ni[P(OEt)$_3$]$_4$ and SZO_{300} and is denoted as Ni/$SZO_{300\text{-}insitu}$. Isomerization of **1a** proceeded to a good yield and selectivity of **2a** with SZO_{300} (78% yield **2a**, E/Z = 17:1; Table 1 entry 4). The major isomer is the *E*-isomer, which is more thermodynamically stable than the *Z*-isomer. The reaction proceeds easily at room temperature, but we chose to run most reactions at 30 °C to ensure consistent temperature control. We proceeded with SZO_{300} as the acid source for **1a** isomerization. No yield of **2a** or conversion of **1a** was observed under these conditions when nickel or SZO_{300} was excluded from the reaction (Table S2).

As a direct comparison to the homogeneous catalyst, the isomerization of **1a** to **2a** using H_2SO_4 as the acid source provided **2a** in higher yield (86%; Table 1, entry 5) than when SZO_{300} was used (78%; Table 1, entry 4), but the E/Z selectivity was comparable (E/Z = 17:1 for both H_2SO_4 and SZO_{300}). Additional Ni^0 sources were also evaluated, and all gave low yields of product (<5%; Table S2). The catalyst loadings of Ni[P(OEt)$_3$]$_4$ and SZO_{300} were optimized to 3 and 5 mol %, respectively, and Et_2O remained the optimal solvent (Table S2). Under these conditions, **1a** is isomerized to **2a** in 1 h in high yield (83%) and high selectivity (E/Z = 22:1; Table 1, entry 6), exhibiting a similar yield to that of using 3 mol % of H_2SO_4 (86%), but with better *E*-selectivity (E/Z =17:1 for H_2SO_4). Increasing H_2SO_4 loading to 5 mol % gave a lower yield of **2a** (63%) with poor selectivity (E/Z = 11:1; Table 1, entry 7), suggesting that the active Ni catalyst may be decomposing in the presence of this slight excess H_2SO_4, as previously reported.[23,24]

Nafion™ and Amberlyst®-15 are both acidic organic polymers and have been used as supports in heterogeneous catalysis.[25,26,37] Evaluating these materials in place of SZO_{300} under our conditions revealed that they are not as effective as SZO_{300}. Nafion™ was the worst-performing acid, yielding 10% **2a** (E/Z = 15:1; Table 1, entry 8), and

Amberlyst®-15 gave slightly higher yield (20% yield; *E*/*Z* = 11:1; Table 1, entry 9). The reactions using three acidic supports (SZO_{300}, Nafion™, and Amberlyst®-15) and H_2SO_4 were studied more deeply by analyzing the reaction progress over time. The plot of the yield of **2c** over time using the three solid acids shows linear formation of the product from 0-45 min (Figure S15). The slopes of these linear portions were calculated, and comparing these slopes shows that the Ni/$SZO_{300\text{-insitu}}$ catalyst is 5 and 11 times faster than the Ni/Amberlyst®-15 and Ni/Nafion™ catalysts, respectively (Figure S15).

Table 1. Evaluation of acid sources for the isomerization of 1a to 2a.

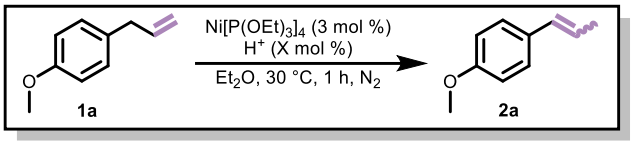

Entry	Acid Source (mol %)		Yield	Selectivity (*E*/*Z*)
1	$SiO_{2\text{-}700}$	(3)	0%	n.d.[a]
2	$Al_2O_{3\text{-}700}$	(3)	0%	n.d.
3	$ZrO_{2\text{-}700}$	(3)	0%	n.d.
4	SZO_{300}	(3)	78%	17:1
5	H_2SO_4	(3)	86%	17:1
6	SZO_{300}	(5)	83%	22:1
7[b]	H_2SO_4	(5)	63%	11:1
8	Nafion™	(5)	10%	15:1
9	Amberlyst®-15	(5)	20%	11:1

Conditions: **1a** (0.060 mmol, 1.0 equiv), $Ni[P(OEt)_3]_4$ (0.0018 mmol, 3.0 mol %), Et_2O (1.0 mL). Yields and selectivities determined by gas chromatography (GC) analysis using cyclooctane as an internal standard. [a]n.d., not determined. [b]**1a** (0.12 mmol, 1.0 equiv), $Ni[P(OEt)_3]_4$ (0.0060 mmol, 5.0 mol %), Et_2O (2.0 mL).

Catalyst Characterization. To quantify the amount of the Ni complex that grafts onto SZO_{300}, a grafting reaction between $Ni[P(OEt)_3]_4$ and SZO_{300} was performed using the same ratio of Ni/acid sites as used in catalysis (3:5). This reaction was performed by gently stirring $Ni[P(OEt)_3]_4$ (0.0187 mmol) and SZO_{300} (0.0300 mmol H^+) in Et_2O for 1.5 h at 23 °C. A stark color change from white (SZO_{300}) to bright orange (grafted material, Ni/$SZO_{300\text{-grafted}}$) was immediately observed upon introducing the colorless solution of $Ni[P(OEt)_3]_4$ to SZO_{300}, visually indicating that a reaction on the surface had occurred (Figure 1d, bottom right). $^{31}P\{^1H\}$ NMR analysis of the reaction filtrate in C_6D_6 revealed that approximately 81% of $Ni[P(OEt)_3]_4$ successfully grafted onto SZO_{300} using 3:5 Ni/$SZO_{300\text{-grafted}}$ (see Supporting Information for details). Ni/$SZO_{300\text{-grafted}}$ was evaluated as a catalyst for isomerization of **1c**; monitoring the reaction over time shows that the conversion of **1c** and *E*/*Z* selectivity of product **2c** was nearly identical to the data obtained with the in situ-generated catalyst (Figures S26-27). Therefore, we conclude that the active catalyst is the same whether the catalyst is formed by grafting and isolating or by generating it in situ.

Upon isolation, the surface organometallic complex, Ni/$SZO_{300\text{-grafted}}$ (6.38 wt % Ni by ICP-MS), was characterized by solid-state NMR spectroscopy (Figure 2). As expected, the ^1H MAS NMR spectrum showcases signals corresponding to Ni-bound $P(OEt)_3$ at 4.09 and 1.28 ppm. Two additional signals further upfield exhibit characteristic hydride resonances at -12.10 and -14.21 ppm, indicating that $Ni[P(OEt)_3]_4$ is indeed protonated by SZO_{300} (Figure 2, top right). The peak at -14.21 ppm aligns with the Ni–H peak in the analogous homogeneous complex, $HNi[P(OEt)_3]_4[HSO_4]$, which appears at -14.3 ppm (τ = 24.3, $J_{P,H}$ = 26.5 Hz) in CD_2Cl_2.[23] This was further supported by forming this homogeneous $[Ni–H]^+$ species under our conditions: a reaction of 1.0 equiv $Ni[P(OEt)_3]_4$ and 1.7 equiv H_2SO_4 in 1:5 C_6D_6/Et_2O was monitored by ^1H, $^{13}C\{^1H\}$, and $^{31}P\{^1H\}$ NMR at 25 °C. The ^1H NMR gave rise to a quintet at -14.34 ppm ($J_{P,H}$ = 26.9 Hz), corroborating the formation of $HNi[P(OEt)_3]_4[HSO_4]$. The appearance of the hydride signal at -12.10 ppm is hypothesized to correspond to $HNi[P(OEt)_3]_4$ interacting with the zirconium oxide bridges on the SZO_{300} surface, resulting in a slight shift downfield. Additionally, other late transition metal-hydride complexes prepared via SOMC methods are commonly found within this region.[38,39] The IR spectrum of Ni/$SZO_{300\text{-grafted}}$ further corroborates the presence of a Ni–H in the grafted material as indicated by a weak band at 1935 cm^{-1}. This data is consistent with previously reported $[Ni–H]^+$ complexes, including the analogous homogeneous system, whose Ni–H stretch is at 1970 cm^{-1}.[23,40,41] The ^{13}C MAS NMR spectrum of Ni/$SZO_{300\text{-grafted}}$ exhibits two peaks at 61.8 and 15.5 ppm that corresponds to the coordinated $P(OEt)_3$ ligands (Figure 2, bottom left), which align with the $^{13}C\{^1H\}$ peaks of $HNi[P(OEt)_3]_4[HSO_4]$ taken in 1:5 C_6D_6/Et_2O at 61.8 and 16.3 ppm (Figure S30). Lastly, a single resonance at 134.28 ppm was observed in the ^{31}P MAS NMR spectrum (Figure 2, bottom right), which is not only significantly upfield compared to that of $Ni[P(OEt)_3]_4$ at 159.23 ppm (taken in C_6D_6), but it also aligns well with the $^{31}P\{^1H\}$ NMR spectrum of $HNi[P(OEt)_3]_4[HSO_4]$ taken in 1:5 C_6D_6/Et_2O, which is a doublet at 132.42 ppm (Figure S31). Overall, these data point towards the protonation of $Ni[P(OEt)_3]_4$ by SZO_{300} to form $[Ni–H]^+$ species on the surface.

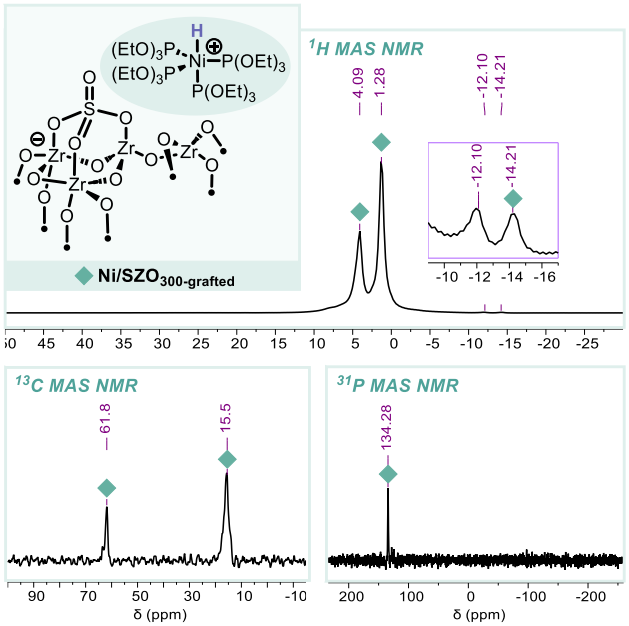

Figure 2. ^1H, ^{13}C, and ^{31}P MAS NMR Characterization of the grafted catalyst, Ni/$SZO_{300\text{-grafted}}$ (teal diamonds).

As SZO_{300} is postulated to protonate $Ni[P(OEt)_3]_4$ to form the desired $[Ni–H]^+$ species, we sought to further understand the acidic nature of SZO_{300} and Ni/$SZO_{300\text{-grafted}}$

through pyridine adsorption studies. This was accomplished by reacting 1.0 equiv of SZO_{300} (based on mmol of surface OH) or $Ni/SZO_{300\text{-grafted}}$ (based on mmol of Ni) with 1.7 equiv of pyridine followed by thermal treatment to remove any adsorbed pyridine on the surface. Diffuse Reflectance Infrared Fourier Transform (DRIFTS) analysis reveals the formation of pyridinium ions in both SZO_{300} and $Ni/SZO_{300\text{-grafted}}$ samples, supporting the Bronsted acidic nature of the unreacted H^+ sites on the surface. This finding alludes to the highly acidic nature of SZO_{300} and its susceptibility to protonate $Ni[P(OEt)_3]_4$ to access a $[Ni–H]^+$ on the surface.

Catalyst Heterogeneity, Stability, Robustness, and Practicality. To investigate the heterogeneity of the catalyst, a hot-filtration test was conducted using $Ni/SZO_{300\text{-grafted}}$. Using standard reaction conditions, two experiments with **1a** were run in parallel, and the reaction progress was monitored over time (Figure 3b). The standard conditions and procedure were used for one reaction (Figure 3b, green diamonds); the other reaction was filtered through a PTFE syringe filter while at 23 °C after 20 minutes and the reaction progress of the filtrate was monitored for an additional 100 minutes (Figure 3b, orange triangles). Heterogeneously catalyzed isomerization will cease after filtration, and if the active catalyst is leaching from the surface to form a homogeneous catalyst in situ, the concentration of product will keep increasing. However, as anticipated, the filtered reaction stagnated, with no additional conversion of **1a**, formation of **2a**, or change in the *E*/*Z* ratio (Figure S40). This key finding supports the notion that this catalyst is heterogeneous in nature. ICP-MS analysis of the reaction filtrate showed 6% of the Ni is in solution. The presence of Ni in solution could be due to remaining physisorbed $Ni[P(OEt)_3]_4$ being desorbed under catalytic reaction conditions or the solid catalyst breaking down by the stir bar and thereby releasing Ni into solution. Despite the presence of Ni in solution, the results of the hot filtration tests and recyclability studies (*vide infra*) suggest that this soluble Ni is not an active catalyst for isomerization and that the active catalyst is heterogeneous. This inactivity of the Ni in solution is likely due to the lack of acid in solution, which would be required to form the active $[Ni–H]^+$ catalyst.

After validating the heterogeneity of the catalyst, we investigated catalyst stability. Tolman found that the active catalyst generated from $Ni[P(OEt)_3]_4$ and H_2SO_4 is highly unstable, converting just 22% of 1-butene after aging the catalyst for 85 minutes, whereas 95% of 1-butene was converted when using freshly prepared catalyst.[22,24] He showed that this catalyst deactivation is due to the reaction between an acid (either excess H_2SO_4 or the counterion HSO_4^-, which forms after protonation of Ni^0) and the proposed active catalyst $[Ni–H]^+$, generating H_2 and an inactive Ni^{II} complex.[23] We hypothesized that the low surface densities of acidic sites on SZO_{300} and the coulombic attraction of the $[Ni–H]^+$ site to the surface anions are effectively immobilizing and localizing the active site, thereby preventing the $[Ni–H]^+$ species from reacting with other acid sites and undergoing this detrimental deactivation pathway.

To test this hypothesis and compare the stabilities of both the $Ni/SZO_{300\text{-insitu}}$ and Ni/H_2SO_4 catalysts, both catalysts were generated and aged in Et_2O for 24 hours, and then their isomerization activity was compared to the activity of freshly prepared catalyst. Figure 4a shows the reaction progress over time for both catalysts and both freshly generated and aged catalysts using allylbenzene (**1c**) as the substrate. The freshly prepared homogeneous catalyst is highly active, reaching quantitative yield before the first aliquot was removed from the reaction for analysis (5 minutes; filled blue squares); aging this catalyst for 24 hours completely deactivates it, and no formation of **2c** is measured after 2 hours (hollow blue squares). The freshly prepared heterogeneous catalyst is slower than fresh Ni/H_2SO_4 (as discussed above for **1a**), reaching 92% yield after 2 hours (filled green diamonds); in contrast to Ni/H_2SO_4, aging $Ni/SZO_{300\text{-insitu}}$ for 24 hours had essentially no impact on the catalyst activity (hollow green diamonds). This stability is also visually observable: both freshly prepared catalysts are bright orange (see Figure 1d for a picture of $Ni/SZO_{300\text{-grafted}}$), but the homogeneous catalyst gradually becomes colorless over the first hour, and the heterogeneous catalyst retains its orange color throughout the 24-hour aging period. These data support our hypothesis that catalyst deactivation is prevented by site-isolating the active site.

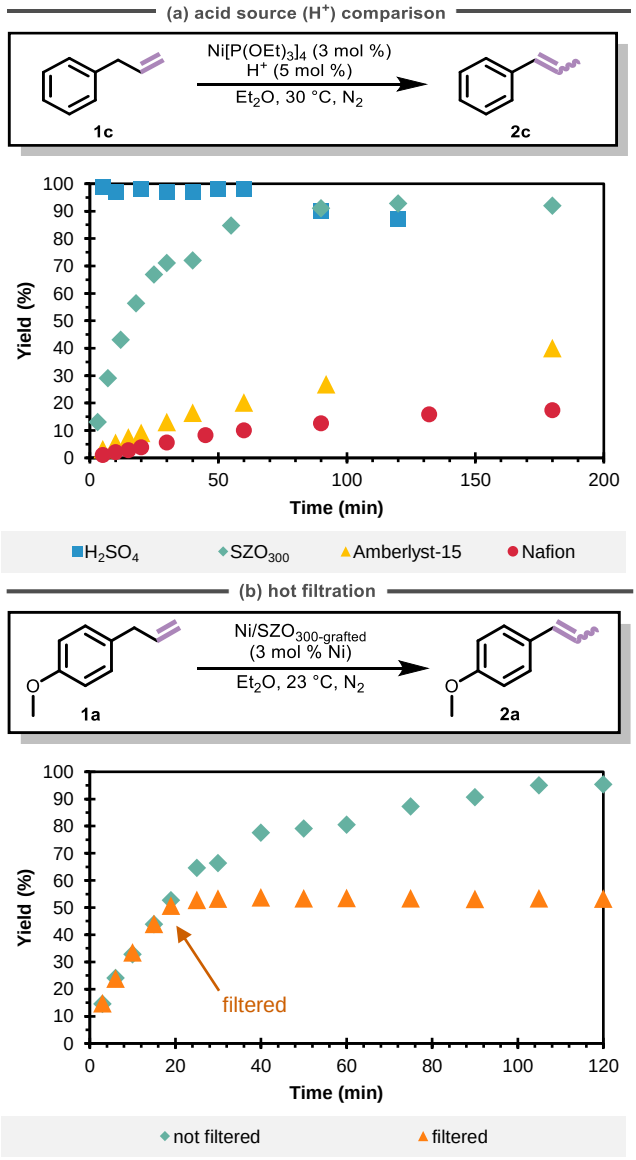

Figure 3. (a) Comparison of the acid sources (H^+) in isomerization of **1c** to **2c**. Conditions: allylbenzene (**1c**, 0.13 mmol, 1.0 equiv), $Ni[P(OEt)_3]_4$ (0.0036 mmol, 3.0 mol %), H^+ (0.0062 mmol, 5.0 mol %), and Et_2O (2.0 mL). (b) Hot-filtration

experiment. Conditions: **1a** (0.12 mmol, 1.0 equiv), Ni/$SZO_{300\text{-grafted}}$ (0.0036 mmol, 3.0 mol % Ni), and Et_2O (2.0 mL). Typical reaction conditions without filtration (green diamonds); filtered reaction (orange triangles). Yield and selectivity determined by GC analysis using cyclooctane as an internal standard for all experiments.

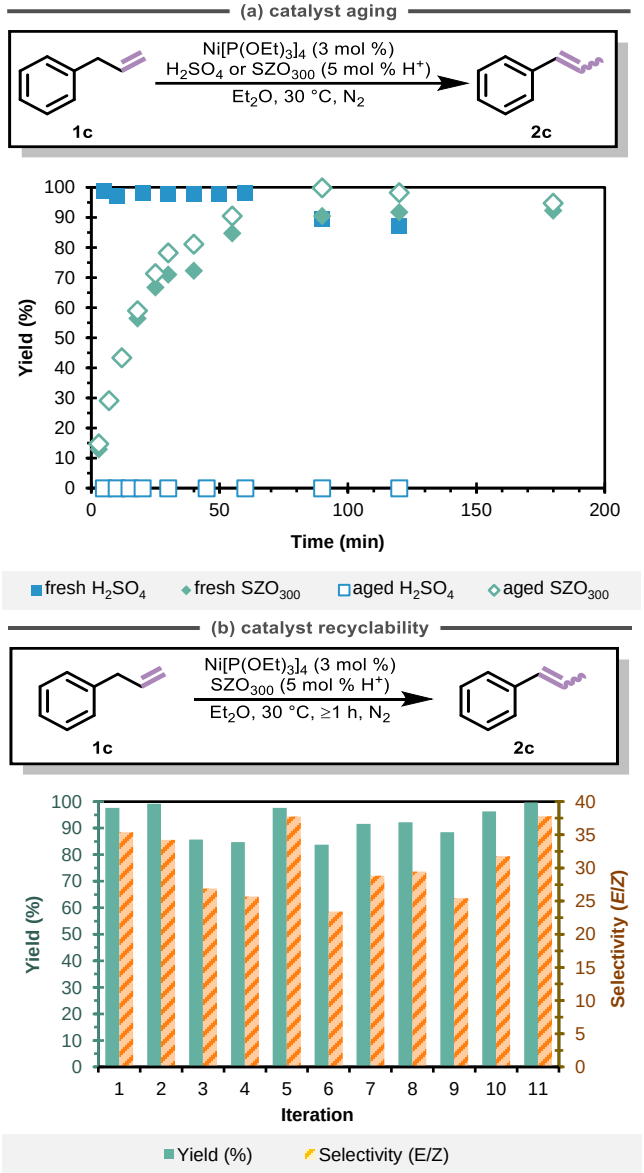

Figure 4. (a) Catalyst aging study of Ni/H_2SO_4 (blue squares) and Ni/$SZO_{300\text{-insitu}}$ (green diamonds). Conditions: **1c** (0.12 mmol, 1.0 equiv), $Ni[P(OEt)_3]_4$ (0.0036 mmol, 3.0 mol %), H_2SO_4 or SZO_{300} (0.0060 mmol H^+, 5.0 mol %), and Et_2O (2.0 mL). (b) Catalyst recyclability study for the isomerization of **1c**. Conditions: (**1c**, 0.060 mmol), $Ni[P(OEt)_3]_4$ (0.0018 mmol, 3.0 mol %), SZO_{300} (0.0030 mmol H^+, 5.0 mol %), and Et_2O (1.0 mL). Yield and selectivity determined by GC analysis using cyclooctane as an internal standard.

The remarkable stability of the heterogeneous catalyst demonstrated in the catalyst aging study inspired us to investigate the recyclability of the catalyst. After generating the catalyst in Et_2O, allylbenzene (**1c**) was added to the reaction at 23 °C. The reaction was allowed to stir for at least 1 h between each cycle to ensure reaction completion. After the reaction, the solution was decanted from the solid and analyzed by GC; then fresh solution of **1c** was introduced to the catalyst. This process was repeated for a total of 10 cycles, giving good-to-excellent yields of **2c** (Figure 4b, left axis) and excellent *E*/*Z* selectivity (Figure 4b, right axis) with little to no catalyst decomposition observed between each cycle (Figure 4b). Variations in *E*/*Z* selectivity were observed between each cycle and are likely a product of the amount of time that the catalyst was allowed to react with **1c**, as increasing the reaction time increases *E*-selectivity (see Supporting Information for details).

Substrate Scope. Having good evidence demonstrating the heterogeneity and high activity of Ni/$SZO_{300\text{-insitu}}$, and using our optimized reaction conditions, we tested a library of alkenes to demonstrate the broadness of the substrate scope (Figure 5). All reactions were performed using 3 mol % $Ni[P(OEt)_3]_4$, 5 mol % H^+ sites in SZO_{300}, Et_2O as the solvent, and 30 °C reaction temperature, unless stated otherwise. We initially evaluated a variety of functional groups using the additive screening protocol (Table S3)[42] and used those results as a guide in substrate choice. A wide range of electronically (**1a**-**1g**) varied akenes were well-tolerated, resulting in good-to-excellent yield (77-94%) and selectivity (*E*/*Z* ≥ 25:1). Adding steric bulk, as seen in substrate **1h**, does not diminish the yield (97%), but the selectivity does decrease to 13:1 (*E*/*Z*). The formation of trisubstituted alkenes in high *E*/*Z* selectivity is a significant challenge in base metal-catalyzed alkene isomerization, with notable advancements using Co and Fe homogeneous catalysts recently disclosed.[43–50] Isomerization of **1i**, a 1,1-disubstituted alkene, to **2i**, a trisubstituted alkene, gave 97% yield and modest selectivity (*E*/*Z* = 7.7:1).

We hypothesized that having a slight molar excess of acidic sites relative to Ni (5 mol % and 3 mol %, respectively) under our optimized conditions might lead to intolerance of acid-sensitive functional groups. However, they are compatible, suggesting that the remaining acidic sites are inaccessible. Substrates with a methoxy methyl ether (**2j**) and trimethylsilyl ether (**2k**) were well-tolerated, giving 68% and 93% yield and 19:1 and 18:1 *E*/*Z* ratios, respectively. Substrates with functional groups that would typically deactivate late transition metal catalysts like phenol (**1l**; 98% yield; *E*/*Z* = >99:1), nitrile (**1m**; 98% yield; *E*/*Z* = 25:1), and carboxylic acid (**1n;** 74% yield; *E*/*Z* = >99:1) are tolerated very well, giving excellent yield and *E*/*Z* selectivity.

Heterocyclic substrates are also tolerated: the indole derivative **1o** yields 70% of **2o** and thiophenes **1p** and **1q** yield 88% of **2p** and 98% of **2q**, respectively. However, the presence of a sulfone in **1r** was not as well-tolerated, with only 37% of **1r** converting to **2r**. The reaction of allylthiophene **1p** did not complete at 30 °C (~60% conversion was measured) but increasing the catalyst loading to 4:7 mol % $Ni[P(OEt)_3]_4/SZO_{300}$, the reaction temperature to 50 °C, and the reaction time to 24 h gave full conversion, and **2p** was isolated in 88% yield. The *E*/*Z* selectivity of products **2o** and **2p** is good, although lower than allylbenzene derivatives (9.5:1 and 7.4:1, respectively). The selectivity of the reaction forming product **2q** reverses, favoring the *Z*-isomer (*E*/*Z* = 1:1.7). The switch in selectivity to favor formation of the *Z* isomer is also seen in phenyl allyl ether **2s** (73% yield; *E*/*Z* = 1:2.8). The *E*- and Z-isomers of enol ethers are known to have similar thermodynamic stabilities.[51–53] Other challenging functional groups with heteroatoms are excellently tolerated. In addition to the amino functional

group in **1o**, the tosyl-protected allyl amine **1t** and the amide **1u** both proceed to high yield (97% and 91%, respectively) and *E*/*Z* selectivity (24:1 and >99:1, respectively). The allyl boronic ester **1v** isomerized to the vinyl boronic ester **2v** in 61% yield and 8.8:1 *E*/*Z* selectivity. Protected phenol derivatives **1w** and **1x** gave excellent yields and *E*/*Z* selectivity (97% and >99% yield; *E*/*Z* = 16:1 and 29:1, respectively). The presence of (pseudo)halides and halides in **1x** and **1y**, respectively, were well tolerated to yield >99% and 92%, respectively, and high selectivity (*E*/*Z* = 29:1 and >99:1, respectively). **1q**, **1x**, and **1y** exemplify the compatibility of halides and (pseudo)halides with these catalytic conditions, holding potential for future derivatization. Likewise, the aldehyde in **1g** was compatible with these reaction conditions, affording the alkene isomerization product **2g** in 94% yield and >99:1 *E*/*Z* selectivity.

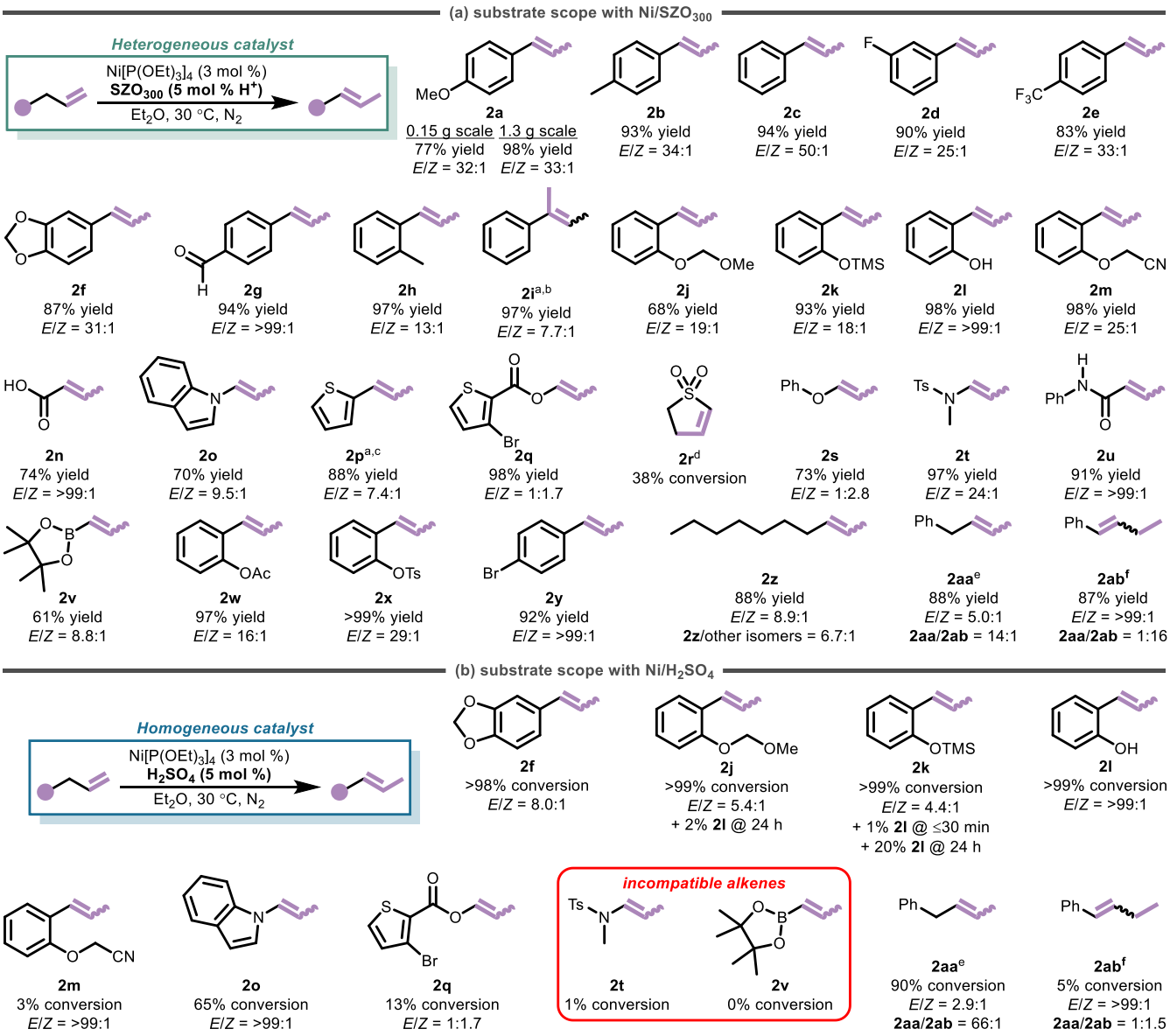

Figure 5. (a) Substrate scope for isomerization using Ni/$SZO_{300\text{-insitu}}$. Isolated yields and selectivity (*E*/*Z*) of the isolated products are reported. The selectivity was determined by relative integrations in the ^{1}H NMR. Conditions: **1** (1.0 mmol, 1.0 equiv), $Ni[P(OEt)_3]_4$ (0.030 mmol, 3.0 mol %), SZO_{300} (0.050 mmol H^+, 5.0 mol %), Et_2O (17 mL), 30 °C, 1-24 h. (b) Substrate scope with Ni/H_2SO_4. Conversion is reported as % conversion to product. Conversion and selectivity were determined by GC or GC-MS. Conditions: **1** (0.060 mmol), $Ni[P(OEt)_3]_4$ (0.0018 mmol, 3.0 mol %), H_2SO_4 (0.0030 mmol H^+, 5 mol %), Et_2O (1.0 mL). Ts, tosyl; TMS, trimethylsilane, Ac, acyl. [a]50 °C. [b]0.87 mmol **1i**, 3.4 mol % $Ni[P(OEt)_3]_4$, 5.6 mol % SZO_{300}. [c]0.68 mmol **1p**, 4.4 mol % $Ni[P(OEt)_3]_4$, 7.4 mol % SZO_{300}. [d]Isolated as a mixture of **1r** and **2r**. [e]0 °C. [f]70 °C.

1-Decene **1z** is readily isomerized to 2-decene **2z** in 88% yield with good selectivity (*E*/*Z* = 8.9:1) and a 6.7:1 ratio of the 2-decene to the 3-, 4-, and 5-decene isomers, demonstrating good positional selectivity. We hypothesized that the good positional selectivity favoring 2-decene over other internal isomers is because internal, *E*-alkenes are less favorable ligands than terminal alkenes[54], leading to faster dissociation of 2-decene from Ni than migratory insertion of 2-decene into the Ni–H bond. To test this hypothesis, an experiment was designed to assess the relative isomerization rates of a **1aa** to **2aa** and of **2aa** to **2ab** using GC analysis (Figure S6). We chose substrates **1aa** and **2aa** because they are easily isolable, unlike the isomers of decene. Taking the linear portion of the first 10 min for each

reaction, the isomerization of **1aa** to **2aa** is 55x faster than the isomerization of **2aa** to **2ab** (Figure S7). These data support our hypothesis and offers a plausible reason for the positional selectivity of decene isomerization. Knowing that the isomerization of a terminal alkene is much faster than isomerization of an internal alkene, we were inspired to evaluate the potential of controlling the positional selectivity of Ni/$SZO_{300\text{-insitu}}$. Using a lower reaction temperature of 0 °C, migration of the alkene in homoallylbenzene **1aa** was controlled to one bond, and **2aa** was formed in 88% yield, 5.0:1 *E*/*Z* selectivity, and 14:1 positional selectivity (**2aa**/**2ab**). Using an elevated temperature (70 °C), alkene migration proceeded to the most thermodynamically favorable site, forming β-ethylstyrene **2ab** in 87% yield, >99:1 *E*/*Z* selectivity, and 1:16 positional selectivity (**2aa**/**2ab**).

To show the practicality of this Ni/$SZO_{300\text{-insitu}}$ catalyst, we performed the isomerization of **1a** on a 1.26 g scale (8.53 mmol) under optimized reaction conditions. **1a** proceeded to complete conversion to **2a** after 2 h. The product was purified by a simple filtration to remove the solid catalyst and concentration to give product **2a**. This straightforward process gave an excellent isolated yield of 98% (1.24 g, 8.37 mmol) while retaining high *E*/*Z* selectivity of 33:1 (*E*/*Z*). These results paired with the diverse functional group tolerance showcase the potential usefulness of this heterogeneous [Ni–H]$^+$ isomerization catalyst.

As an effort to simply the system, $Zr(OH)_4$•*n*H_2SO_4, which is the synthetic precursor to SZO_{300}, was evaluated as a viable acid source for alkene isomerization. Under standard reaction conditions, $Zr(OH)_4$•*n*H_2SO_4 was used in place of SZO_{300} for the isomerization of **1t**, an alkene that was incompatible with the homogeneous catalyst. After 24 h, ^{1}H NMR analysis of the crude reaction indicates 9% of unreacted **1t**, 65% of **2t** with low *E*/*Z* selectivty of 6.2:1 (*E*/*Z*), as well as deallylated **1t** to form TsN(Me)H, **S1** (compare to the results with Ni/$SZO_{300\text{-insitu}}$: *E*/*Z* = 24:1, 97% yield, no deallylation observed). Both Ni and Pd have been previously reported to deallylate amines.[55,56] Although the isomerization of **1t** is observed using Ni/$Zr(OH)_4$•*n*H_2SO_4, the low *E*/*Z* selectivity and the competing side reaction deem this catalytic system less effective than the Ni/$SZO_{300\text{-insitu}}$ system. This indicates that SZO_{300} is indeed required for broadly applicable alkene isomerization activity, stereoselectivity, and chemoselectivity.

Comparison of Ni/$SZO_{300\text{-insitu}}$ to Homogeneous Catalysts. A subset of the substrates included in Figure 5a were also evaluated for isomerization using Ni/H_2SO_4, the homogeneous analog of Ni/SZO_{300}, using standard conditions (Figure 5b). With a few exceptions, we found that the heterogeneous Ni/$SZO_{300\text{-insitu}}$ catalyst is generally more compatible with more functional groups and is more selective. Substrates **1t** and **1v** are incompatible with Ni/H_2SO_4 (≤1% conversion), and substrates **1m** and **1q** give very low conversions to the isomerized product (3% and 13%, respectively), but all of these substrates give excellent yields with Ni/$SZO_{300\text{-insitu}}$ (97%, 61%, 98%, and 98%, respectively). Notably, we have not found a substrate that is compatible with Ni/H_2SO_4 and incompatible with the heterogeneous Ni/$SZO_{300\text{-insitu}}$ catalyst, highlighting the unique advantages offered by this heterogeneous catalyst. Ni/H_2SO_4 outcompeted Ni/$SZO_{300\text{-insitu}}$ with only one identified substrate, **1l**: >99% conversion and >99:1 *E*/*Z* selectivity in <30 min with Ni/H_2SO_4, 98% yield and >99:1 *E*/*Z* selectivity in 4 h with Ni/$SZO_{300\text{-insitu}}$. Ni/H_2SO_4 took 24 hours to catalyze **1o** to **2o** in 65% conversion with an *E*/*Z* ratio of >99:1, but this substrate reached complete conversion (70% isolated yield) and *E*/*Z* ratio of 9.5:1 (*E*/*Z*) in just 8 hours with Ni/$SZO_{300\text{-insitu}}$. Conversion of **1f, 1j,** and **1k** using Ni/H_2SO_4 was high (≥98% for all) after less than 30 minutes, while the Ni/$SZO_{300\text{-insitu}}$ catalyst required 5-8 hours to reach similar conversion. However, for these alkenes **1f**, **1j,** and **1k** the *E*/*Z* selectivity with Ni/$SZO_{300\text{-insitu}}$ (31:1, 19:1, and 18:1, respectively) was significantly better than with Ni/H_2SO_4 (8.0:1, 5.4:1, 4.4:1, respectively). Further demonstrating the advantage of using Ni/$SZO_{300\text{-insitu}}$ over its homogeneous analog, the deprotected phenol (**2l**) was observed after just 30 minutes of reaction time with substrate **1k**, and after 24 h, 20% **2l** was formed. Deprotection was also observed with substrate **1j**. No evidence of deprotection was present with Ni/$SZO_{300\text{-insitu}}$. We next investigated the positional selectivity of the Ni/H_2SO_4 system. At 0 °C, 90% **1aa** was converted to **2aa** with improved positional selectivity (**2aa/2ab** = 66:1) but with diminished *E*-selectivity (*E*/*Z* = 2.9:1) in comparison to the Ni/$SZO_{300\text{-insitu}}$ system (**2aa/2ab** = 14:1, *E*/*Z* = 5.0:1). On the contrary, the Ni/H_2SO_4 catalyst was rather unstable at 70 °C revealed by the low conversion of **1aa** to **2ab** (5%) and poor positional selectivity (**2aa**/**2ab** = 1:1.5). These results further show the advantages of having enhanced catalyst stability, seen in the Ni/$SZO_{300\text{-insitu}}$ system, compared to the much less stable homogeneous analog.

To further demonstrate the exceptional performance of Ni/$SZO_{300\text{-insitu}}$, we sought to compare its activity and selectivity to those from other state-of-the-art homogeneous Ni and Pd catalysts (Figure 6). Schoenebeck,[57] Engle and Vantourout,[58] our lab,[59] and others[4,47–52] have recently developed Ni-catalyzed isomerization catalysts that are *E*-selective. Additionally, Skrydstrup reported a Pd-catalyzed isomerization system that is highly active and compatible with a diverse set of alkene-containing substrates.[66] Despite the rich display of reactivity exhibited by these homogeneous catalysts, minimal work has been done to unveil relative isomerization rates.

We initiated our studies by monitoring the formation of **2a** from **1a** over time for the following systems: Ni$[P(OEt)_3]_4$/SZO_{300} (**A**; this work); $(IPr)_2Ni_2Cl_2$ (**B**; Schoenebeck;[57] IPr = 1,3-bis(2,6-diisopropylphenyl)imidazol-2-ylidene), Ni$(cod)_2$/PCy_3•HBF_4, (**C**; Engle and Vantourout;[58] cod = cyclooctadiene; Cy = cyclohexyl), (IPr)Ni(hex)/$HSiPh_3$, (**D**; Cook;[59] hex = 1,5-hexadiene), and Pd$(dba)_2$/P(*t*-Bu)$_3$/*i*-PrC(O)Cl (**E**; Skrydstrup;[66] dba = dibenzoylacetone). Each isomerization reaction was performed under its respective optimized conditions and the product formation over time was measured by GC (Figure 6).

Monitoring the reactions over time, we see that all but system **D** (Figure 6, yellow triangles) reach completion by 180 min. Due to the induction periods observed for systems **C** and **D**, linear rates were not calculated to compare relative isomerization rates between each system. Visual analysis of the reaction progress over time reveal that systems **B**, **C**, and **D** all exhibit slower reaction kinetics than **A** and **E**. It is notable that system **A** (Ni/$SZO_{300\text{-insitu}}$) is performed at 30 °C using 3 mol % Ni, while system **E** requires an elevated reaction temperature of 80 °C, but performs well using just 0.5 mol % Pd. The corresponding selectivity

profiles for systems **C**, **D**, and **E** all equilibrate to ~15:1 (*E*/*Z*) at 3 h, whereas systems **A** and **B** gradually increase over time to ~30:1 *E*/*Z* by 3 h (Figure S61). These catalyst systems were also all compared at equal catalyst loadings (3 mol % Ni or Pd and 3 mol % additive/ligand) and reaction temperature (30 °C), but with each respective system's optimal reaction solvent and concentration (Figures S62-63). Ni/$SZO_{300\text{-insitu}}$ reaches completion in ~90 min (91% yield), systems **B**, **D**, and **E** reach ~20% conversion after 150 min, and system **C** does not produce any product. Ni/$SZO_{300\text{-insitu}}$ also reaches the highest selectivity after 2 h compared to the other catalysts. These data further demonstrate the excellent performance of Ni/$SZO_{300\text{-insitu}}$, even in comparison to the state-of-the-art Ni and Pd catalysts.

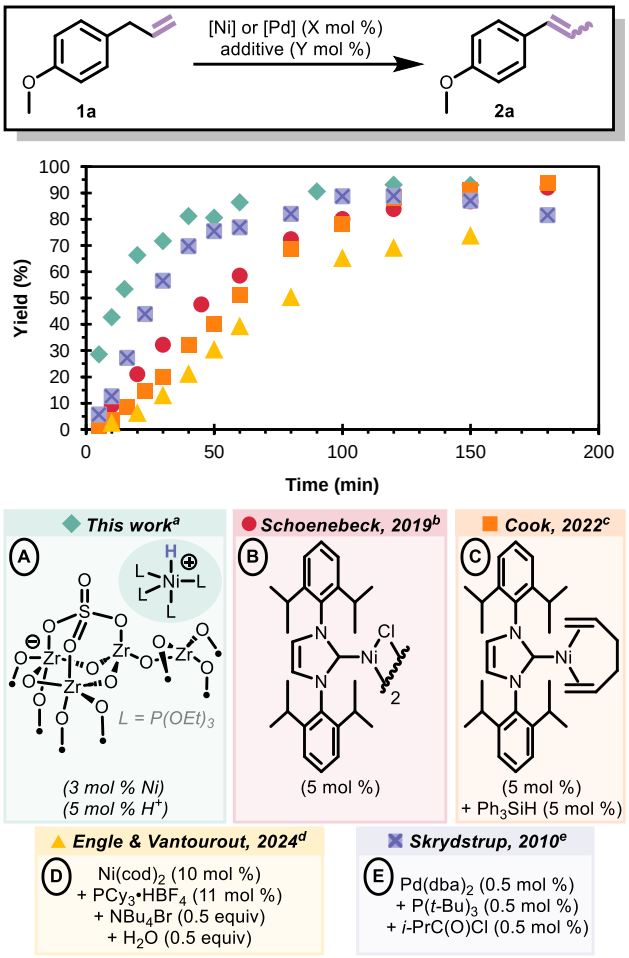

Figure 6. Kinetic analysis of Ni and Pd isomerization catalysts. **1a** (0.12 mmol unless otherwise stated). [a]Ni[P(OEt)$_3$]$_4$ (0.0036 mmol, 3.0 mol %), SZO_{300} (0.0060 mmol H$^+$, 5.0 mol %), Et_2O (2.0 mL), 23 °C. [b]$(IPr)_2Ni_2Cl_2$ (0.0060 mmol, 5.0 mol %), ClC_6H_5 (0.3 mL), 30 °C. [c](IPr)Ni(hex) (0.0060 mmol, 5.0 mol %), $HSiPh_3$ (0.0061 mmol, 5.0 mol %), hexanes (0.38 mL), 80 °C. [d]**1a** (0.25 mmol), $Ni(cod)_2$ (0.025 mmol, 10 mol %), PCy_3•HBF_4 (0.027 mmol, 11 mol %), NBu_4Br (0.12 mmol), H_2O (0.12 mmol), DMF (5.0 mL), 30 °C. [e]$Pd(dba)_2$ (0.00061 mmol, 0.50 mol %), P(*t*-Bu)$_3$ (0.00061 mmol, 0.50 mol %), *i*-PrC(O)Cl (0.00061 mmol, 0.50 mol %), toluene (2.9 mL), 80 °C. IPr, (IPr = 1,3-bis(2,6-diisopropylphenyl)imidazol-2-ylidene); cod, 1,5-cyclooctadiene; hex, 1,5-hexadiene; dba, dibenzylideneacetone.

Mechanistic Studies. Having successfully developed a heterogeneous isomerization catalyst with a large substrate scope, we embarked on preliminary mechanistic investigations. We hypothesized that the heterogeneous catalyst has similar reaction and catalyst activation mechanisms as the Ni/H_2SO_4 catalyst. Alkene isomerization most often occurs via 1) a radical mechanism, 2) $C_{allylic}$–H activation to form a metal-allyl intermediate, and 3) M–H (M = metal) insertion/elimination pathways.[1–5] Tolman demonstrated that the homogeneous Ni/H_2SO_4 catalyst proceeds though a M–H insertion/elimination pathway,[24] so we hypothesized that Ni/$SZO_{300\text{-insitu}}$ would operate under the same mechanism. To probe whether a radical pathway is occurring, we tested the reaction of Ni/$SZO_{300\text{-insitu}}$ with **1ac** (Scheme 1a). If isomerization proceeds through a radical pathway, a few rearrangement products are possible.[43,67,68] However, none of these rearrangement products were observed at 30 °C, 50 °C, and 70 °C, implying that a radical pathway is not proceeding. As an additional radical probe, the 1,6-diene **1ad**, which is expected to cyclize to form a methylenecyclopentane under radical conditions, shows only alkene isomerization with Ni/$SZO_{300\text{-insitu}}$ (Scheme 1b). After reacting **1ad** for 5 h at 30 °C, 97% of **1ad** was converted to the 1,5-diene (**2ad**), and no trace of cyclized product was identified by GC or ^{1}H NMR analysis, further confirming that this reaction is likely not going through a radical pathway.[59,69]

Scheme 1. Mechanistic experiments. (a) Reactivity with vinyl cyclopropane (**1ac**). (b) Reactivity with a 1,6-diene (**1ad**). (c) Reactivity with a vinyl cyclopropane (**1ae**). (d) Crossover experiment between **1a** and **1c-*d*$_n$**.

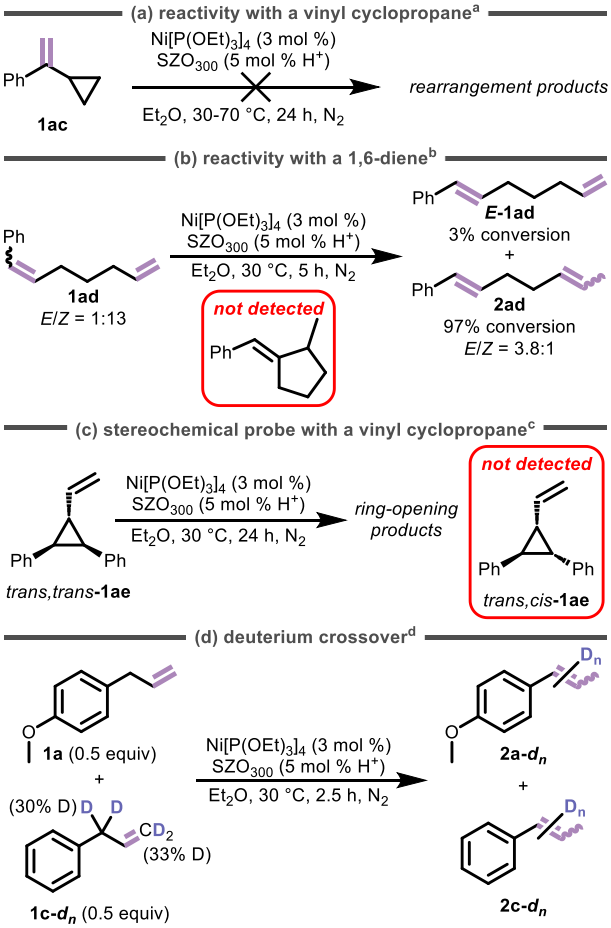

[a]Conditions: **1ac** (0.060 mmol), Ni[P(OEt)$_3$]$_4$ (0.0018 mmol, 3.0 mol %), SZO_{300} (0.0030 mmol H$^+$, 5.0 mol %), Et_2O (1.0 mL). [b]Conditions: **1ad** (1.0 mmol), Ni[P(OEt)$_3$]$_4$ (0.030 mmol, 3.0 mol %), SZO_{300} (0.050 mmol H$^+$, 5.0 mol %), Et_2O (17 mL). [c]

Conditions: **1ae** (0.066 mmol), Ni[P(OEt)$_3$]$_4$ (0.0020 mmol, 3.0 mol %), SZO$_{300}$ (0.0033 mmol H$^+$, 5.0 mol %), Et$_2$O (1.1 mL). [d]**1a** (0.28 mmol, 0.50 equiv), **1c-*d*$_n$** (0.28 mmol, 0.50 equiv), Ni[P(OEt)$_3$]$_4$ (0.017 mmol, 3.0 mol %), SZO$_{300}$ (0.028 mmol H$^+$, 5.0 mol %), Et$_2$O (9.6 mL).

In our last mechanistic experiment to probe if a radical route is operative, the vinyl cyclopropane (**1ae**) was reacted with Ni/SZO$_{300\text{-insitu}}$ under standard reaction conditions for 24 h.[57] Vinyl cyclopropanes are highly sensitive to radical-mediated reversible ring-opening and can undergo a *trans–cis* isomerization/rearrangement.[70,71] If a radical mechanism was operative with Ni/SZO$_{300\text{-insitu}}$, then *cis-trans* isomerization is expected, and no reaction is expected if the mechanism proceeds via two-electron pathways. GC-MS, ^{1}H and ^{13}C{^{1}H} NMR analysis of the reaction revealed unreacted **1ae** (75%) and ring-opening products (25%). Most importantly, no evidence of the rearranged product (*trans,cis*-**1ae**) was observed, suggesting that a radical mechanism is not occurring.

We next wanted to distinguish between an allyl (intramolecular) or Ni–H insertion-elimination (intermolecular) mechanism. A crossover experiment was performed with 0.5 equiv **1a** and 0.5 equiv **1c-*d*$_n$** (Scheme 1d). If an allyl pathway is occurring, no protium/deuterium scrambling between the two substrates is expected.[2] Deuterium incorporation into **2a** and protium incorporation into **2c-*d*$_n$** is predicted if the mechanism proceeds via a Ni–H insertion/elimination mechanism, since the Ni–H/D formed during the reaction could exchange one alkene ligand for another. Analysis of the ^{1}H and ^{2}H NMR spectra revealed significant protium/deuterium scrambling in both **2a** and **2c-*d*$_n$**, supporting the viability of an intermolecular, Ni–H insertion-elimination pathway (Figures S48-S51).

Potential of Ni/SZO$_{300\text{-insitu}}$ in Additional Catalytic Reactions. As metal–hydrides are often invoked in catalysis, our final goal is to demonstrate the broad utility of this heterogeneous catalyst by evaluating its activity in other catalytic reactions. Metal-catalyzed alkene hydrofunctionalization reactions offer access to value-added chemicals by installing structural diversity.[72–76] Specifically, hydroalkenylation is utilized in the Shell higher olefin process to produce 1x10^6 tons of olefins annually.[77] Additionally, hydroboration[78,79] products are excellent Suzuki-Miyaura cross-coupling partners to construct C–C bonds in organic synthesis.[80–82] Hydrosilylation reactions produce valuable organosilicon compounds used in reactions like Hiyama couplings for C–C bond formation,[83,83] Tamao-Fleming oxidations to form alcohols,[84–87] and polymerizations to form silicone materials[88–90]

Ni/SZO$_{300\text{-insitu}}$ is a viable catalyst for hydroalkenylation, hydroboration, and hydrosilylation of alkenes (Figure 7). Notably, the results of these Ni/SZO$_{300\text{-insitu}}$-catalyzed reactions are unoptimized. Ni/SZO$_{300\text{-insitu}}$ is an excellent styrene hydroalkenylation catalyst, affording 94% yield (determined ^{1}H NMR spectroscopy using an internal standard) of product **3a**, with no evidence of formation of the other hydrovinylation isomers. Hydroboration[91,92] of the vinyl amide **2u** using B$_2$pin$_2$, LiO*t*-Bu, and MeOH resulted in 55% yield of product **3b** (determined by GCMS using an internal standard); like hydrovinylation, this reaction is highly selective, and product **3b** is the only isomer observed by both GC-MS and ^{1}H NMR spectroscopy. Lastly, styrene is hydrosilylated[93] by Ph$_2$SiH$_2$ using catalyst Ni/SZO$_{300\text{-insitu}}$, giving 21% yield of **3c** in 7:1 selectivity (branched/linear), as determined by GC using an internal standard. These results demonstrate the potential for broad utility that this novel heterogeneous catalyst, Ni/SZO$_{300\text{-insitu}}$, holds.

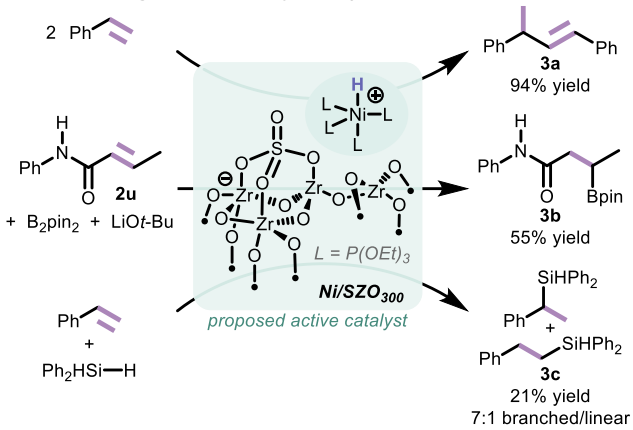

Figure 7. [Ni–H]$^+$-catalyzed reactions under unoptimized conditions. Hydroalkenylation of styrene to afford **3a** (top). Hydroboration of **2u** and B$_2$Pin$_2$ to afford **3b** (middle). Hydrosilylation of styrene and H$_2$SiPh$_2$ to afford **3c** (bottom).

CONCLUSION

The combination of Ni[P(OEt)$_3$]$_4$ and SZO$_{300}$ generates a potent alkene isomerization catalyst, with marked improvement over previous work that used sulfated polymers to heterogenize the Ni[P(OEt)$_3$]$_4$/H$^+$ isomerization system. Ni/SZO$_{300\text{-insitu}}$ is heterogeneous in nature, as demonstrated by a hot-filtration test, and is highly recyclable and robust, as demonstrated with catalyst aging studies. Characterization of the solid catalyst shows the presence of a Ni–H and Ni-bound P(OEt)$_3$ ligands, which support the hypothesis that [{OEt)$_3$P}$_4$Ni–H]$^+$ is the active site. We presume that the active site is bound to the support via an ionic bond between the cationic Ni complex and the anionic support, but a more thorough investigation into the nature of this interaction is required to confirm this conclusion. Remarkably, the substrate scope is very broad and includes various heteroatoms, acid-labile groups, halides, carboxylic acids, and amides. The catalyst can also be kinetically controlled to achieve specific positional isomers when using a long chain alkene. Preliminary mechanistic results suggest against radical and allyl pathways but do allude to a M–H insertion/elimination mechanism for alkene isomerization. Ni/SZO$_{300\text{-insitu}}$ also outcompetes state-of-the-art homogeneous Ni and Pd catalysts in head-to-head comparisons, in terms of both reaction rates and selectivity. The rational approach to designing this active site led to a heterogeneous catalyst with significantly increased catalyst versatility over its homogeneous counterpart.

ASSOCIATED CONTENT

Details on synthetic procedures, characterization of products, kinetics data, and NMR, IR, HRMS characterization are included in the supporting information. This material is available free of charge via the Internet at http://pubs.acs.org.

AUTHOR INFORMATION

Corresponding Author

Amanda K. Cook – Department of Chemistry and Biochemistry, University of Oregon, Eugene, Oregon 97403, United States; orcid.org/0000-0003-3501-8502; Email: akcook@uoregon.edu

Authors

Alison Sy-min Chang – Department of Chemistry and Biochemistry, University of Oregon, Eugene, Oregon 97403, United States

Melanie A. Kascoutas – Department of Chemistry and Biochemistry, University of Oregon, Eugene, Oregon 97403, United States

Quinn P. Valentine – Department of Chemistry and Biochemistry, University of Oregon, Eugene, Oregon 97403, United States

Kiera I. How – Department of Chemistry and Biochemistry, University of Oregon, Eugene, Oregon 97403, United States

Rachel M. Thomas – Department of Chemistry and Biochemistry, University of Oregon, Eugene, Oregon 97403, United States. Current address: Department of Chemistry, University of Illinois Urbana-Champaign, Champaign, Illinois 61820, United States

Notes

The authors declare no competing financial interest.

ACKNOWLEDGMENTS

This research was supported by the Office of the Vice President of Research and the College of Arts and Sciences at the University of Oregon. The National Science Foundation supported part of this work through the CAREER award CHE-2238379. A.S.C. acknowledges the NSF for a GRFP fellowship. R.M.T. acknowledges the NSF for an REU Summer Fellowship (CHE-1659346). The authors would like to thank Anastasiia Konovalova and Shannon Boettcher for providing Nafion™, Liam Twight for ICP-MS assistance, and Audrey Davenport for DRIFTS and DRUV-vis assistance.

REFERENCES

(1) Kochi, T.; Kanno, S.; Kakiuchi, F. Nondissociative Chain Walking as a Strategy in Catalytic Organic Synthesis. *Tetrahedron Letters* **2019**, *60* (37), 150938. https://doi.org/10.1016/j.tetlet.2019.07.029.

(2) Massad, I.; Marek, I. Alkene Isomerization through Allylmetals as a Strategic Tool in Stereoselective Synthesis. *ACS Catal.* **2020**, *10* (10), 5793–5804. https://doi.org/10.1021/acscatal.0c01174.

(3) Larionov, E.; Li, H.; Mazet, C. Well-Defined Transition Metal Hydrides in Catalytic Isomerizations. *Chem. Commun.* **2014**, *50* (69), 9816–9826. https://doi.org/10.1039/C4CC02399D.

(4) Liu, X. L., Bin; Liu, Qiang. Base-Metal-Catalyzed Olefin Isomerization Reactions. *Synthesis* **2019**, *51* (06), 1293–1310. https://doi.org/10.1055/s-0037-1612014.

(5) Molloy, J. J.; Morack, T.; Gilmour, R. Positional and Geometrical Isomerisation of Alkenes: The Pinnacle of Atom Economy. *Angewandte Chemie International Edition* **2019**, *58* (39), 13654–13664. https://doi.org/10.1002/anie.201906124.

(6) Dumesic, J. A.; Huber, G. W.; Boudart, M. Principles of Heterogeneous Catalysis. In *Handbook of Heterogeneous Catalysis*; 2008. https://doi.org/10.1002/9783527610044.hetcat0001.

(7) Cui, X.; Li, W.; Ryabchuk, P.; Junge, K.; Beller, M. Bridging Homogeneous and Heterogeneous Catalysis by Heterogeneous Single-Metal-Site Catalysts. *Nature Catalysis* **2018**, *1* (6), 385–397. https://doi.org/10.1038/s41929-018-0090-9.

(8) Baxendale, I. R.; Lee, A.-L.; Ley, S. V. A Concise Synthesis of Carpanone Using Solid-Supported Reagents and Scavengers. *J. Chem. Soc., Perkin Trans. 1* **2002**, No. 16, 1850–1857. https://doi.org/10.1039/B203388G.

(9) Larsen, C. R.; Paulson, E. R.; Erdogan, G.; Grotjahn, D. B. A Facile, Convenient, and Green Route to (E)-Propenylbenzene Flavors and Fragrances by Alkene Isomerization. *Synlett* **2015**, *26* (17), 2462–2466. https://doi.org/10.1055/s-0035-1560205.

(10) Liu, Z.; Song, J.; Zhang, Y.; Sun, S.; Kun, Z.; Chen, J.; Xie, C.; Jia, X. A Rh-Catalyzed Isomerization of 1-Alkenes to (E)-2-Alkenes: From a Homogeneous Rh/PPh3 Catalyst to a Heterogeneous Rh/POP-PPh3-SO3Na Catalyst. *Catal. Sci. Technol.* **2023**, *13* (4), 963–967. https://doi.org/10.1039/D2CY02016E.

(11) Dunning, H. N. Review of Olefin Isomerization. *Ind. Eng. Chem.* **1953**, *45* (3), 551–564. https://doi.org/10.1021/ie50519a029.

(12) Chuc, L. T. N.; Chen, C.-S.; Lo, W.-S.; Shen, P.-C.; Hsuan, Y.-C.; Tsai, H.-H. G.; Shieh, F.-K.; Hou, D.-R. Long-Range Olefin Isomerization Catalyzed by Palladium(0) Nanoparticles. *ACS Omega* **2017**, *2* (2), 698–711. https://doi.org/10.1021/acsomega.6b00509.

(13) Copéret, C.; Chabanas, M.; Petroff Saint-Arroman, R.; Basset, J.-M. Homogeneous and Heterogeneous Catalysis: Bridging the Gap through Surface Organometallic Chemistry. *Angewandte Chemie International Edition* **2003**, *42* (2), 156–181. https://doi.org/10.1002/anie.200390072.

(14) Copéret, C.; Comas-Vives, A.; Conley, M. P.; Estes, D. P.; Fedorov, A.; Mougel, V.; Nagae, H.; Núñez-Zarur, F.; Zhizhko, P. A. Surface Organometallic and Coordination Chemistry toward Single-Site Heterogeneous Catalysts: Strategies, Methods, Structures, and Activities. *Chem. Rev.* **2016**, *116* (2), 323–421. https://doi.org/10.1021/acs.chemrev.5b00373.

(15) Maier, S.; Cronin, S. P.; Vu Dinh, M.-A.; Li, Z.; Dyballa, M.; Nowakowski, M.; Bauer, M.; Estes, D. P. Immobilized Platinum Hydride Species as Catalysts for Olefin Isomerizations and Enyne Cycloisomerizations. *Organometallics* **2021**, *40* (11), 1751–1757. https://doi.org/10.1021/acs.organomet.1c00216.

(16) Desai, S. P.; Ye, J.; Zheng, J.; Ferrandon, M. S.; Webber, T. E.; Platero-Prats, A. E.; Duan, J.; Garcia-Holley, P.; Camaioni, D. M.; Chapman, K. W.; Delferro, M.; Farha, O. K.; Fulton, J. L.; Gagliardi, L.; Lercher, J. A.; Penn, R. L.; Stein, A.; Lu, C. C. Well-Defined Rhodium–Gallium Catalytic Sites in a Metal–Organic Framework: Promoter-Controlled Selectivity in Alkyne Semihydrogenation to E-Alkenes. *J. Am. Chem. Soc.* **2018**, *140* (45), 15309–15318. https://doi.org/10.1021/jacs.8b08550.

(17) Sheng, D.; Zhang, Y.; Song, Q.; Xu, G.; Peng, D.; Hou, H.; Xie, R.; Shan, D.; Liu, P. Isomerization of 1-Butene to 2-Butene Catalyzed by Metal–Organic Frameworks. *Organometallics* **2020**, *39* (1), 51–57. https://doi.org/10.1021/acs.organomet.9b00599.

(18) Hicks, K. E.; Wolek, A. T. Y.; Farha, O. K.; Notestein, J. M. The Dependence of Olefin Hydrogenation and Isomerization Rates on Zirconium Metal–Organic Framework Structure. *ACS Catal.* **2022**, *12* (21), 13671–13680. https://doi.org/10.1021/acscatal.2c04303.

(19) Conley, M. P.; Mougel, V.; Peryshkov, D. V.; Forrest, W. P. Jr.; Gajan, D.; Lesage, A.; Emsley, L.; Copéret, C.; Schrock, R. R. A Well-Defined Silica-Supported Tungsten Oxo Alkylidene Is a Highly Active Alkene Metathesis Catalyst. *J.*

Am. Chem. Soc. **2013**, *135* (51), 19068–19070. https://doi.org/10.1021/ja410052u.

(20) Staples, O.; Ferrandon, M. S.; Laurent, G. P.; Kanbur, U.; Kropf, A. J.; Gau, M. R.; Carroll, P. J.; McCullough, K.; Sorsche, D.; Perras, F. A.; Delferro, M.; Kaphan, D. M.; Mindiola, D. J. Silica Supported Organometallic IrI Complexes Enable Efficient Catalytic Methane Borylation. *J. Am. Chem. Soc.* **2023**, *145* (14), 7992–8000. https://doi.org/10.1021/jacs.2c13612.

(21) Zhang, J.; Mason, A. H.; Motta, A.; Cesar, L. G.; Kratish, Y.; Lohr, T. L.; Miller, J. T.; Gao, Y.; Marks, T. J. Surface vs Homogeneous Organo-Hafnium Catalyst Ion-Pairing and Ligand Effects on Ethylene Homo- and Copolymerizations. *ACS Catal.* **2021**, *11* (6), 3239–3250. https://doi.org/10.1021/acscatal.0c04678.

(22) Cramer, R.; Lindsey, R. V. Jr. The Mechanism of Isomerization of Olefins with Transition Metal Catalysts. *J. Am. Chem. Soc.* **1966**, *88* (15), 3534–3544. https://doi.org/10.1021/ja00967a013.

(23) Tolman, C. A. Chemistry of Tetrakis(Triethyl Phosphite) Nickel Hydride, HNi[P(OEt)3]4+. I. Nickel Hydride Formation and Decay. *J. Am. Chem. Soc.* **1970**, *92* (14), 4217–4222. https://doi.org/10.1021/ja00717a015.

(24) Tolman, C. A. Chemistry of Tetrakis(Triethyl Phosphite)Nickel Hydride, HNi[P(OEt)3]4+. IV. Mechanism of Olefin Isomerization. *J. Am. Chem. Soc.* **1972**, *94* (9), 2994–2999. https://doi.org/10.1021/ja00764a016.

(25) Hodges, A. M.; Linton, M.; Mau, A. W.-H.; Cavell, K. J.; Hey, J. A.; Seen, A. J. Perfluorinated Membranes as Catalyst Supports. *Applied Organometallic Chemistry* **1990**, *4* (5), 465–473. https://doi.org/10.1002/aoc.590040507.

(26) Raje, A. P.; Datta, R. Activity and Stability of Ion-Exchange Resin-Supported Tetrakis(Triethyl Phosphite)Nickel Hydride Catalyst: Vapor Phase Isomerization of n-Butene. *Journal of Molecular Catalysis* **1992**, *72* (1), 97–116. https://doi.org/10.1016/0304-5102(92)80034-E.

(27) Witzke, R. J.; Chapovetsky, A.; Conley, M. P.; Kaphan, D. M.; Delferro, M. Nontraditional Catalyst Supports in Surface Organometallic Chemistry. *ACS Catal.* **2020**, *10* (20), 11822–11840. https://doi.org/10.1021/acscatal.0c03350.

(28) Samudrala, K. K.; Conley, M. P. Effects of Surface Acidity on the Structure of Organometallics Supported on Oxide Surfaces. *Chem. Commun.* **2023**, *59* (28), 4115–4127. https://doi.org/10.1039/D3CC00047H.

(29) Stalzer, M. M.; Nicholas, C. P.; Bhattacharyya, A.; Motta, A.; Delferro, M.; Marks, T. J. Single-Face/All-Cis Arene Hydrogenation by a Supported Single-Site D0 Organozirconium Catalyst. *Angewandte Chemie International Edition* **2016**, *55* (17), 5263–5267. https://doi.org/10.1002/anie.201600345.

(30) Syed, Z. H.; Kaphan, D. M.; Perras, F. A.; Pruski, M.; Ferrandon, M. S.; Wegener, E. C.; Celik, G.; Wen, J.; Liu, C.; Dogan, F.; Goldberg, K. I.; Delferro, M. Electrophilic Organoiridium(III) Pincer Complexes on Sulfated Zirconia for Hydrocarbon Activation and Functionalization. *J. Am. Chem. Soc.* **2019**, *141* (15), 6325–6337. https://doi.org/10.1021/jacs.9b00896.

(31) Tafazolian, H.; Culver, D. B.; Conley, M. P. A Well-Defined Ni(II) α-Diimine Catalyst Supported on Sulfated Zirconia for Polymerization Catalysis. *Organometallics* **2017**, *36* (13), 2385–2388. https://doi.org/10.1021/acs.organomet.7b00402.

(32) Culver, D. B.; Tafazolian, H.; Conley, M. P. A Bulky Pd(II) α-Diimine Catalyst Supported on Sulfated Zirconia for the Polymerization of Ethylene and Copolymerization of Ethylene and Methyl Acrylate. *Organometallics* **2018**, *37* (6), 1001–1006. https://doi.org/10.1021/acs.organomet.8b00016.

(33) Klet, R. C.; Kaphan, D. M.; Liu, C.; Yang, C.; Kropf, A. J.; Perras, F. A.; Pruski, M.; Hock, A. S.; Delferro, M. Evidence for Redox Mechanisms in Organometallic Chemisorption and Reactivity on Sulfated Metal Oxides. *J. Am. Chem. Soc.* **2018**, *140* (20), 6308–6316. https://doi.org/10.1021/jacs.8b00995.

(34) Kaphan, D. M.; Klet, R. C.; Perras, F. A.; Pruski, M.; Yang, C.; Kropf, A. J.; Delferro, M. Surface Organometallic Chemistry of Supported Iridium(III) as a Probe for Organotransition Metal–Support Interactions in C–H Activation. *ACS Catal.* **2018**, *8* (6), 5363–5373. https://doi.org/10.1021/acscatal.8b00855.

(35) Gao, J.; Zhu, L.; Conley, M. P. Cationic Tantalum Hydrides Catalyze Hydrogenolysis and Alkane Metathesis Reactions of Paraffins and Polyethylene. *J. Am. Chem. Soc.* **2023**, *145* (9), 4964–4968. https://doi.org/10.1021/jacs.2c13610.

(36) Hino, M.; Arata, K. Synthesis of Solid Superacid Catalyst with Acid Strength of H0⩽–16.04. *J. Chem. Soc., Chem. Commun.* **1980**, No. 18, 851–852. https://doi.org/10.1039/C39800000851.

(37) Seen, A. J. Nafion: An Excellent Support for Metal-Complex Catalysts. *Journal of Molecular Catalysis A: Chemical* **2001**, *177* (1), 105–112. https://doi.org/10.1016/S1381-1169(01)00312-0.

(38) Berthoud, R.; Baudouin, A.; Fenet, B.; Lukens, W.; Pelzer, K.; Basset, J.-M.; Candy, J.-P.; Copéret, C. Mononuclear Ruthenium Hydride Species versus Ruthenium Nanoparticles: The Effect of Silane Functionalities on Silica Surfaces. *Chemistry – A European Journal* **2008**, *14* (12), 3523–3526. https://doi.org/10.1002/chem.200800174.

(39) Rimoldi, M.; Fodor, D.; van Bokhoven, J. A.; Mezzetti, A. A Stable 16-Electron Iridium(Iii) Hydride Complex Grafted on SBA-15: A Single-Site Catalyst for Alkene Hydrogenation. *Chem. Commun.* **2013**, *49* (96), 11314–11316. https://doi.org/10.1039/C3CC47296E.

(40) Imoto, H.; Moriyama, H.; Saito, T.; Sasaki, Y. Synthesis of Cationic Hydride and Related Complexes of Palladium and Nickel with Tricyclohexylphosphine or Triisopropylphosphine. *Journal of Organometallic Chemistry* **1976**, *120* (3), 453–460. https://doi.org/10.1016/S0022-328X(00)98056-2.

(41) Tenorio, M. J.; Puerta, M. C.; Valerga, P. Synthesis and Characterisation of a Novel Nickel Trihydride. Crystal Structure of [{Ni(Dippe)}2H3][BPh4](Dippe = Pri2PCH2CH2PPri2). *J. Chem. Soc., Dalton Trans.* **1996**, No. 7, 1305–1308. https://doi.org/10.1039/DT9960001305.

(42) Collins, K. D.; Glorius, F. Intermolecular Reaction Screening as a Tool for Reaction Evaluation. *Acc. Chem. Res.* **2015**, *48* (3), 619–627. https://doi.org/10.1021/ar500434f.

(43) Crossley, S. W. M.; Barabé, F.; Shenvi, R. A. Simple, Chemoselective, Catalytic Olefin Isomerization. *J. Am. Chem. Soc.* **2014**, *136* (48), 16788–16791. https://doi.org/10.1021/ja5105602.

(44) Li, G.; Kuo, J. L.; Han, A.; Abuyuan, J. M.; Young, L. C.; Norton, J. R.; Palmer, J. H. Radical Isomerization and Cycloisomerization Initiated by H• Transfer. *J. Am. Chem. Soc.* **2016**, *138* (24), 7698–7704. https://doi.org/10.1021/jacs.6b03509.

(45) Liu, X.; Zhang, W.; Wang, Y.; Zhang, Z.-X.; Jiao, L.; Liu, Q. Cobalt-Catalyzed Regioselective Olefin Isomerization Under Kinetic Control. *J. Am. Chem. Soc.* **2018**, *140* (22), 6873–6882. https://doi.org/10.1021/jacs.8b01815.

(46) Zhang, S.; Bedi, D.; Cheng, L.; Unruh, D. K.; Li, G.; Findlater, M. Cobalt(II)-Catalyzed Stereoselective Olefin Isomerization: Facile Access to Acyclic Trisubstituted Alkenes. *J. Am. Chem. Soc.* **2020**, *142* (19), 8910–8917. https://doi.org/10.1021/jacs.0c02101.

(47) Liu, H.; Cai, C.; Ding, Y.; Chen, J.; Liu, B.; Xia, Y. Cobalt-Catalyzed E-Selective Isomerization of Alkenes with a Phosphine-Amido-Oxazoline Ligand. *ACS Omega* **2020**, *5* (20), 11655–11670. https://doi.org/10.1021/acsomega.0c00951.

(48) Yu, X.; Zhao, H.; Li, P.; Koh, M. J. Iron-Catalyzed Tunable and Site-Selective Olefin Transposition. *J. Am. Chem. Soc.* **2020**, *142* (42), 18223–18230. https://doi.org/10.1021/jacs.0c08631.

(49) Xu, S.; Geng, P.; Li, Y.; Liu, G.; Zhang, L.; Guo, Y.; Huang, Z. Pincer Iron Hydride Complexes for Alkene Isomerization: Catalytic Approach to Trisubstituted (Z)-Alkenyl Boronates. *ACS Catal.* **2021**, *11* (16), 10138–10147. https://doi.org/10.1021/acscatal.1c02432.

(50) Xu, S.; Liu, G.; Huang, Z. Iron Catalyzed Isomerization of α-Alkyl Styrenes to Access Trisubstituted Alkenes. *Chinese Journal of Chemistry* **2021**, *39* (3), 585–589. https://doi.org/10.1002/cjoc.202000492.

(51) Larsen, C. R.; Grotjahn, D. B. Stereoselective Alkene Isomerization over One Position. *J. Am. Chem. Soc.* **2012**, *134* (25), 10357–10360. https://doi.org/10.1021/ja3036477.

(52) Kinetic Control via Chelation through the Oxygen Is Also a Possibility. See Ref 53.

(53) Clark, H. C.; Kurosawa, H. Chemistry of Hydrides. XV. Mechanism of Double-Bond Migration Induced by Platinum(II) Hydrides. *Inorg. Chem.* **1973**, *12* (7), 1566–1569. https://doi.org/10.1021/ic50125a018.

(54) Tolman, C. A. Olefin Complexes of Nickel(0). III. Formation Constants of (Olefin)Bis(Tri-o-Tolyl Phosphite)Nickel Complexes. *J. Am. Chem. Soc.* **1974**, *96* (9), 2780–2789. https://doi.org/10.1021/ja00816a020.

(55) Lemaire-Audoire, S.; Savignac, M.; Genêt, J. P.; Bernard, J.-M. Selective Deprotection of Allyl Amines Using Palladium. *Tetrahedron Letters* **1995**, *36* (8), 1267–1270. https://doi.org/10.1016/0040-4039(95)00003-U.

(56) Bao, L.; Liang, H.; Zhang, H.; Yan, Z.; Sun, C.; Pang, S. Polystyrene-Supported Nickel Complex Catalysed Deprotection of Allylic Tertiary Amine with Sodium Borohydride. *IOP Conference Series: Materials Science and Engineering* **2020**, *772* (1), 012101. https://doi.org/10.1088/1757-899X/772/1/012101.

(57) Kapat, A.; Sperger, T.; Guven, S.; Schoenebeck, F. E-Olefins through Intramolecular Radical Relocation. *Science* **2019**, *363* (6425), 391–396. https://doi.org/10.1126/science.aav1610.

(58) Rubel, C.; Ravn, A.; Yang, S.; Li, Z.-Q.; Engle, K.; Vantourout, J. Stereodivergent, Kinetically Controlled Isomerization of Terminal Alkenes via Nickel Catalysis. *Angew. Chem. Int. Ed.* **2024**, 63, e202320081. https://doi.org/10.1002/anie.202320081.

(59) Kawamura, K. E.; Chang, A. S.; Martin, D. J.; Smith, H. M.; Morris, P. T.; Cook, A. K. Modular Ni(0)/Silane Catalytic System for the Isomerization of Alkenes. *Organometallics* **2022**, *41* (4), 486–496. https://doi.org/10.1021/acs.organomet.2c00010.

(60) Saputra, L.; Arifin; Gustini, N.; Sinambela, N.; Indriyani, N. P.; Sakti, A. W.; Arrozi, U. S. F.; Martoprawiro, M. A.; Patah, A.; Permana, Y. Nitrile Modulated-Ni(0) Phosphines in Trans-Selective Phenylpropenoids Isomerization: An Allylic Route by a Regular H1-N(End-on) or an Alkyl Route via a Flipped-Nitrile? *Molecular Catalysis* **2022**, *533*, 112768. https://doi.org/10.1016/j.mcat.2022.112768.

(61) Huang, L.; Lim, E. Q.; Koh, M. J. Secondary Phosphine Oxide-Activated Nickel Catalysts for Site-Selective Alkene Isomerization and Remote Hydrophosphination. *Chem Catalysis* **2022**, *2* (3), 508–518. https://doi.org/10.1016/j.checat.2021.12.014.

(62) Tricoire, M.; Wang, D.; Rajeshkumar, T.; Maron, L.; Danoun, G.; Nocton, G. Electron Shuttle in N-Heteroaromatic Ni Catalysts for Alkene Isomerization. *JACS Au* **2022**, *2* (8), 1881–1888. https://doi.org/10.1021/jacsau.2c00251.

(63) Cruz, T. F. C.; Lopes, P. S.; Gomes, P. T. Allylnickel(II) Complexes of Bulky 5-Substituted-2-Iminopyrrolyl Ligands. *Polyhedron* **2021**, *207*, 115357. https://doi.org/10.1016/j.poly.2021.115357.

(64) Iwamoto, H.; Tsuruta, T.; Ogoshi, S. Development and Mechanistic Studies of (E)-Selective Isomerization/Tandem Hydroarylation Reactions of Alkenes with a Nickel(0)/Phosphine Catalyst. *ACS Catal.* **2021**, *11* (11), 6741–6749. https://doi.org/10.1021/acscatal.1c00908.

(65) Kathe, P. M.; Caciuleanu, A.; Berkefeld, A.; Fleischer, I. Tandem Olefin Isomerization/Cyclization Catalyzed by Complex Nickel Hydride and Brønsted Acid. *J. Org. Chem.* **2020**, *85* (23), 15183–15196. https://doi.org/10.1021/acs.joc.0c02033.

(66) Gauthier, D.; Lindhardt, A. T.; Olsen, E. P. K.; Overgaard, J.; Skrydstrup, T. In Situ Generated Bulky Palladium Hydride Complexes as Catalysts for the Efficient Isomerization of Olefins. Selective Transformation of Terminal Alkenes to 2-Alkenes. *J. Am. Chem. Soc.* **2010**, *132* (23), 7998–8009. https://doi.org/10.1021/ja9108424.

(67) Bullock, R. M.; Samsel, E. G. Hydrogen Atom Transfer Reactions of Transition-Metal Hydrides. Utilization of a Radical Rearrangement in the Determination of Hydrogen Atom Transfer Rates. *J. Am. Chem. Soc.* **1987**, *109* (21), 6542–6544. https://doi.org/10.1021/ja00255a067.

(68) Liu, Y.; Wang, Q.-L.; Chen, Z.; Zhou, C.-S.; Xiong, B.-Q.; Zhang, P.-L.; Yang, C.-A.; Zhou, Q. Oxidative Radical Ring-Opening/Cyclization of Cyclopropane Derivatives. *Beilstein J. Org. Chem.* **2019**, *15*, 256–278. https://doi.org/10.3762/bjoc.15.23.

(69) Zuo, G.; Louie, J. Highly Active Nickel Catalysts for the Isomerization of Unactivated Vinyl Cyclopropanes to Cyclopentenes. *Angewandte Chemie International Edition* **2004**, *43* (17), 2277–2279. https://doi.org/10.1002/anie.200353469.

(70) Tanko, J. M.; Drumright, R. E. Radical Ion Probes. 2. Evidence for the Reversible Ring Opening of Arylcyclopropylketyl Anions. Implications for Mechanistic Studies. *J. Am. Chem. Soc.* **1992**, *114* (5), 1844–1854. https://doi.org/10.1021/ja00031a045.

(71) Choi, S.-Y.; Toy, P. H.; Newcomb, M. Picosecond Radical Kinetics. Fast Ring Openings of Secondary and Tertiary Trans-2-Phenylcyclopropylcarbinyl Radicals. *J. Org. Chem.* **1998**, *63* (23), 8609–8613. https://doi.org/10.1021/jo981020a.

(72) RajanBabu, T. V. Asymmetric Hydrovinylation Reaction. *Chem. Rev.* **2003**, *103* (8), 2845–2860. https://doi.org/10.1021/cr020040g.

(73) RajanBabu, T. V. In Pursuit of an Ideal Carbon-Carbon Bond-Forming Reaction: Development and Applications of the Hydrovinylation of Olefins. *Synlett* **2009**, *2009* (06), 853–885. https://doi.org/10.1055/s-0028-1088213.

(74) Hilt, G. Hydrovinylation Reactions – Atom-Economic Transformations with Steadily Increasing Synthetic Potential. *European Journal of Organic Chemistry* **2012**, *2012* (24), 4441–4451. https://doi.org/10.1002/ejoc.201200212.
(75) Suginome, M.; Ohmura, T. Transition Metal-Catalyzed Element-Boryl Additions to Unsaturated Organic Compounds. In *Boronic Acids*, 2nd ed.; Wiley-VCH Verlag & Co. KGaA, 2011; pp 171–212. https://doi.org/10.1002/9783527639328.ch3.
(76) Marciniec, B. Hydrosilylation of Alkenes and Their Derivatives. In *Hydrosilylation: A Comprehensive Review on Recent Advances*; Marciniec, B., Ed.; Springer Netherlands: Dordrecht, 2009; pp 3–51. https://doi.org/10.1007/978-1-4020-8172-9_1.
(77) Keim, W. Oligomerization of Ethylene to α-Olefins: Discovery and Development of the Shell Higher Olefin Process (SHOP). *Angewandte Chemie International Edition* **2013**, *52* (48), 12492–12496. https://doi.org/10.1002/anie.201305308.
(78) Obligacion, J. V.; Chirik, P. J. Earth-Abundant Transition Metal Catalysts for Alkene Hydrosilylation and Hydroboration. *Nature Reviews Chemistry* **2018**, *2* (5), 15–34. https://doi.org/10.1038/s41570-018-0001-2.
(79) Geier, S. J.; Vogels, C. M.; Melanson, J. A.; Westcott, S. A. The Transition Metal-Catalysed Hydroboration Reaction. *Chem. Soc. Rev.* **2022**, *51* (21), 8877–8922. https://doi.org/10.1039/D2CS00344A.
(80) Miyaura, Norio.; Suzuki, Akira. Palladium-Catalyzed Cross-Coupling Reactions of Organoboron Compounds. *Chem. Rev.* **1995**, *95* (7), 2457–2483. https://doi.org/10.1021/cr00039a007.
(81) Valente, C.; Organ, M. G. The Contemporary Suzuki–Miyaura Reaction. In *Boronic Acids*, 2nd ed.; Wiley-VCH Verlag & Co. KGaA, 2011; pp 213–262. https://doi.org/10.1002/9783527639328.ch4.
(82) Farhang, M.; Akbarzadeh, A. R.; Rabbani, M.; Ghadiri, A. M. A Retrospective-Prospective Review of Suzuki–Miyaura Reaction: From Cross-Coupling Reaction to Pharmaceutical Industry Applications. *Polyhedron* **2022**, *227*, 116124. https://doi.org/10.1016/j.poly.2022.116124.
(83) Nakao, Y.; Hiyama, T. Silicon-Based Cross-Coupling Reaction: An Environmentally Benign Version. *Chem. Soc. Rev.* **2011**, *40* (10), 4893–4901. https://doi.org/10.1039/C1CS15122C.
(84) Jones, G. R.; Landais, Y. The Oxidation of the Carbon-Silicon Bond. *Tetrahedron* **1996**, *52* (22), 7599–7662. https://doi.org/10.1016/S0040-4020(96)00038-5.
(85) Roy, A.; Oestreich, M. At Long Last: The Me3Si Group as a Masked Alcohol. *Angewandte Chemie International Edition* **2021**, *60* (9), 4408–4410. https://doi.org/10.1002/anie.202017157.
(86) Tamao, K.; Ishida, N.; Tanaka, T.; Kumada, M. Silafunctional Compounds in Organic Synthesis. Part 20. Hydrogen Peroxide Oxidation of the Silicon-Carbon Bond in Organoalkoxysilanes. *Organometallics* **1983**, *2* (11), 1694–1696. https://doi.org/10.1021/om50005a041.
(87) Fleming, I.; Henning, R.; Plaut, H. The Phenyldimethylsilyl Group as a Masked Form of the Hydroxy Group. *J. Chem. Soc., Chem. Commun.* **1984**, No. 1, 29–31. https://doi.org/10.1039/C39840000029.
(88) Marciniec, B. Functionalisation and Cross-Linking of Organosilicon Polymers. In *Hydrosilylation: A Comprehensive Review on Recent Advances*; Marciniec, B., Ed.; Springer Netherlands: Dordrecht, 2009; pp 159–189. https://doi.org/10.1007/978-1-4020-8172-9_5.
(89) Marciniec, B. Hydrosilylation Polymerisation. In *Hydrosilylation: A Comprehensive Review on Recent Advances*; Marciniec, B., Ed.; Springer Netherlands: Dordrecht, 2009; pp 191–214. https://doi.org/10.1007/978-1-4020-8172-9_6.
(90) Marciniec, B. Organosilicon – Organic Hybrid Polymers and Materials. In *Hydrosilylation: A Comprehensive Review on Recent Advances*; Marciniec, B., Ed.; Springer Netherlands: Dordrecht, 2009; pp 241–286. https://doi.org/10.1007/978-1-4020-8172-9_8.
(91) Hirano, K.; Yorimitsu, H.; Oshima, K. Nickel-Catalyzed β-Boration of α,β-Unsaturated Esters and Amides with Bis(Pinacolato)Diboron. *Org. Lett.* **2007**, *9* (24), 5031–5033. https://doi.org/10.1021/ol702254g.
(92) Yu, X.; Zhao, H.; Xi, S.; Chen, Z.; Wang, X.; Wang, L.; Lin, L. Q. H.; Loh, K. P.; Koh, M. J. Site-Selective Alkene Borylation Enabled by Synergistic Hydrometallation and Borometallation. *Nature Catalysis* **2020**, *3* (7), 585–592. https://doi.org/10.1038/s41929-020-0470-9.
(93) Chang, A. S.; Kawamura, K. E.; Henness, H. S.; Salpino, V. M.; Greene, J. C.; Zakharov, L. N.; Cook, A. K. (NHC)Ni(0)-Catalyzed Branched-Selective Alkene Hydrosilylation with Secondary and Tertiary Silanes. *ACS Catal.* **2022**, *12* (18), 11002–11014. https://doi.org/10.1021/acscatal.2c03580.

For Table of Contents Only